ARCHIVES OF MECHANICS
Arch. Mech. **74** (2-3), 173–200, 2022, DOI: 10.24423/aom.3955

Reactive solute transport in blood flow through a permeable capillary

S. DEBNATH[1)], A. K. ROY[2)], O. A. BÉG[3)]

[1)] *Division of Mathematics, School of Advanced Sciences, Vellore Institute of Technology, Chennai 600127, India*

[2)] *Department of Science and Humanities, Tripura Institute of Technology, Narsingarh, Tripura 799009, India, rk.ashis10@gmail.com (corresponding author)*

[3)] *Mechanical Engineering Department, School of Science, Engineering and Environment (SEE), University of Salford, Manchester, UK*

The present analysis discusses the solute transport process in a steady 2D (axial and radial) laminar flow of blood through a permeable, finite length capillary. Blood is treated as a homogeneous Newtonian fluid and the solute is absorbed at the capillary wall with a linear irreversible reaction rate. The velocity profile is obtained by a regular perturbation technique, whereas the transport coefficients depicted by the Gill generalized dispersion model are solved numerically. A number of different scenarios are considered, namely transport with no-reaction, weak absorption, strong absorption, low filtration or high filtration, etc. In the initial stages, the temporal behaviour of the dispersion coefficient is identical to those cases when there is no radial velocity. For the combined effect of radial and axial velocities, however, the dispersion coefficient is lower for a high absorption rate than for a weak absorption rate. Diffusion is accelerated with higher values of filtration coefficient. Owing to the opposite effects of radial diffusion and radial velocity, the solute particles require more time to reach the steady state. The analysis finds applications in, for example, reactive nutrient and pharmacological transport in capillary hemodynamics.

Key words: capillary, axial and radial flow, solute dispersion, Gill decomposition, filtration coefficient, exchange coefficient, advection coefficient.

1. Introduction

One of the most vital fluids in the body is blood [1] which has numerous critical functions, the most important of which is to provide oxygen and nutrients to every living cell and to remove various toxic products from each cell. This function is performed by transporting various components of blood across a capillary wall and into the surrounding tissue, as mentioned earlier. The micro-circulation constitutes that component of the circulation system featuring vessels with extremely small diameters, typically less than 150 microns. It includes a number of microcirculatory vessels such as arterioles, capillaries

and venules (capacitance vessels) which together enable many vital functions to be performed including regulation of tissue perfusion, blood-tissue exchange and tissue blood volume. The capillaries are the site of major exchange between blood and tissue [2]. Via capillaries, nutrients and other molecules diffuse or are transported across the capillary wall to sustain life [3]. Capillary walls are made up of a single layer of endothelial cells and have different shapes and sizes depending on the tissue in which they are found. In capillary flows, Starling's hypothesis is important and implies that the rate of flow per unit area through the wall surface is proportional to the difference between the pressure of the fluid within and outside of the capillary [4]. Fung and Zweifach [5] provided an excellent appraisal of Newtonian blood flow in capillaries considering many important geometric characteristics, boundary conditions and Reynolds number ranges. Many excellent analytical and numerical investigations have been conducted of capillary blood flows. These studies have examined many different hemodynamic and geometric aspects including viscosity, hemo-rheology, squeezing of individual blood cells, capillary networks etc. Barnard *et al.* [6] studied the axially symmetric flow of a deformable blood cell in a conduit (capillary) by formulating a non-linear boundary value problem and showed that parachute geometry cells arise which do not impinge on the vessel wall. They also observed that ratio of cell to plasma viscosity is modified when the cell and conduit diameter are of the same order. Secomb *et al.* [7] used a lubrication theory model to analyze the flow of blood cells along a capillary (narrow cylindrical vessel geometry) and included elastic properties of the red blood cell membrane, including shear and bending structural characteristics. They noted that apparent viscosity is elevated with a decrement in flow rate. El-Shahed [8] presented perturbation solutions of for two-phase Newtonian blood flow in a capillary (a suspension of cells in plasma), deriving expressions for velocity and pressure distributions within the tube for a variety of cell concentrations. Fibich *et al.* [9] developed a continuum flow model for blood transport in a long, elastic, and permeable capillary, under external tissue pressure, driven by arteriolar-venular pressure difference. They included the effects of ultrafiltration due to transmural hydrostatic and osmotic gradients. They observed that where tissue pressure is high (e.g., in the subendocardium), the capillary flow experiences substantial periodic volume changes, which generate the intramyocardial pumping. They also demonstrated good correlation of the theoretical results for flow structures with epicardial phasic flow measurements. Soltani and Chen [10] used a finite difference numerical technique to study the interstitial fluid and blood flow in a porous capillary network geometry containing solid tumors. They deployed the Darcy-modified Navier–Stokes equation and considered also intravascular flows, and also considered the adaptability of the capillary diameter to hemodynamics and metabolic stimuli. Peyrounette *et al.* [11] computed the blood flow in a capillary bed, with

a homogenized continuum porous medium approach. They simulated the larger arteriolar and venular trees as a network of interconnected tubes and evaluated accurately the pressure gradients arising in the capillaries connected to arterioles or venules. Motivated by clinical applications in electrophoretic haemotology, Tripathi *et al.* [12] investigated the unsteady electro-kinetic peristaltic transport of blood in cylindrical finite length capillaries. They used a Newtonian lubrication model and the Debye–Hückel linearization (wall zeta potential greatly less than 25 mV) and computed the influence of inverse Debye length) and the Helmholtz–Smoluchowski velocity on the axial velocity, pressure gradient, volumetric flow rate, local wall shear stress and bolus trapping patterns. Many other excellent works (Pozridikis [13], Fedosov *et al.* [14], Boryczko *et al.* [15], McWhirter *et al.* [16], Durrant and Mccammon [17]) on capillary blood flows are also available in the scientific literature.

Mechanistic studies of fluid flow across the capillary wall are important for understanding metabolism [18]. Such transport involves the solute dispersion (e.g., glucose, amino acids, lactic acids and various drug molecules transport in such a context). Dispersion and mass transport in capillary blood flows are fundamental to a number of clinical applications including the evaluation of drug concentration-time profiles in cerebral pharmacology where the drug is subject to distributional and elimination processes including bulk flow of the cerebrospinal fluid (CSF), binding and metabolism, diffusion, bulk flow of the brain extracellular fluid (ECF) and extra-intracellular exchange. Other applications in which mass transport in capillary hemodynamics arises include oxygen transport in cerebro-capillary networks [19], hematological bioprocessing [20], the spreading of tracer particles in high hematocrit blood [21], nutrient (e.g., protein) transport in the capillary-tissue exchange system [22], glycocalyx-lined capillaries in cardiac fluid mechanics [23] and potassium fate in skeletal muscles [24]. Solute transport is achieved via several mechanisms including convection and axial and radial diffusion. As a result, the effective diffusion coefficient (which accounts for both the effects) or the dispersion coefficient, is one of the crucial factors in the solute transport process as it is typically a few orders of magnitude greater than that due to convection. Taylor [25] in his pioneering study, emphasized that at a developed state, the dispersion of a solute along the tube can be treated such that the center of the slug travels with the cross-sectional mean speed of flow (advection velocity), and the slug is diffused with an augmented effective diffusivity (dispersion coefficient) which is a function of the molecular diffusivity and advection velocity. The Taylor dispersion model has been extended and significantly refined by many other authors. The most prominent of these was [26] Aris' work, which included an axial diffusion term to analyse the dispersion process by means of statistical parameters of the solute concentration distribution. There are many articles (Mazumder and Das [27], Mazumder

and Mondal [28], Mazumder and Paul [29], Debnath *et al.* [30–34], Roy *et al.* [35–37], Zhang *et al.* [38], Li *et al.* [39], Debnath and Ghoshal [40], Guan *et al.* [41]) considered Aris's method and discussed the diffusion process with the help of statistical moments. Gill [42] further proposed an alternative approach for finding the transport coefficients using a series expansion technique. The Gill model is known as the generalised dispersion model and has been frequently used in many studies (Sarkar and Jayaraman [43], Nagarani *et al.* [44], Ng and Rudraiah [45], Paul and Ng [46], Jiang *et al.* [47], Debnath *et al.* [48, 49], Rana and Murthy [50, 51], Jiang and Chen [52], Roy and Shaw [53], Guo *et al.* [54]) under several environments. To understand the long-time behaviour of the dispersion coefficient, many authors (Ng [55], Wu and Chen [56], Roy *et al.* [57]) have deployed the homogenization technique. In a recent work, Rana and Murthy [58] have elaborated the dispersion due to the periodic flow of non-Newtonian fluid in a conduit. They have used the generalized dispersion technique and solved the transport coefficients for all times. Very recently, Roy *et al.* [59] have investigated the reactive diffusion and dispersion in permeable vessels with quadratic porous drag (Forchheimer) effects. Other studies on dispersion in blood flows include Roy and Bég [60] (for transient dispersion in stratified Newtonian/micropolar rheological biofluids), Roy and Shaw [53] (who described detailed simulations of drug dispersion in unsteady blood flow through a micro-vessel with wall absorption with a two-fluid rheological formulation), Das *et al.* [61] (on solute dispersion through the Casson fluid flowing in a stenotic tube having an absorptive wall), etc. Recently, Wang *et al.* [62] have studied on the dispersion process of gyrotactic microorganisms suspended in a horizontal Poiseuille flow, which is also relevant to biomedical transport phenomena.

The solution of the equation for the second order term in the Gill series expansion provides the exact formula for the Taylor dispersion coefficient. Furthermore, to realistically appraise solute transport between capillaries and surrounding tissues, the classic Taylor model is restricted to very low Péclet numbers. A more comprehensive approach is required to accurately characterize the dispersion of solute, e.g., pharmacological agents, glucose, albumin etc, in the capillary, at any Péclet number. In capillary hemodynamics with solute dispersion, the exchange and advection coefficients play an important role and must be included to provide a more comprehensive appraisal of transport characteristics. This is the motivation for the present study, which aims to investigate the solute dispersion in a permeable blood vessel, with a generalized dispersion model. Blood is considered to be a Newtonian fluid which is feasible for high shear stress circulatory flows. Unlike earlier studies (Chu *et al.* [63], Nakad *et al.* [64]) of solute dispersion in 2-D flow, the present mathematical model enables a more comprehensive and refined assessment of the dispersion process in hemodynamics. Also,

due to consideration of the endothelium layer encircling the blood vessel, a new parameter, viz., the filtration coefficient, appears in the study naturally, which affects all the transport coefficients.

2. Mathematical formulation

Consider an amount of chemically active solute (e.g., pharmacological agent) of mass, Q^*, which is injected in the bloodstream through a permeable capillary of radius R^* with finite length $2L^*$. The physical model is shown in Fig. 1.

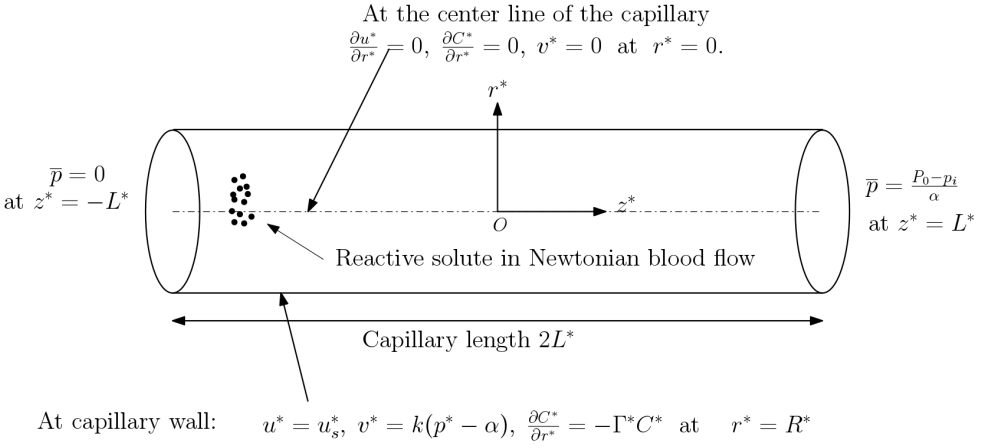

FIG. 1. Axisymmetric rigid permeable capillary blood flow and dispersion model.

Due to the complexity of blood composition in capillary flows, the following assumptions are invoked to enable a simulation of the transport of solute in capillary blood flow:

(i) The capillary tube geometry is cylindrical vessel, which is straight and rigid with uniform cross-section.

(ii) The capillary wall is permeable and has a permeability which follows Starling's law.

(iii) Blood is assumed to be a homogeneous, incompressible, Newtonian fluid with constant density ρ^* and viscosity μ^*. Though, blood exhibits a non-Newtonian behaviour at a low shear rate for small diameter arteries (LONG *et al.* [65], GOLDSMITH and SKALAK [66]); however, the prescription of Newtonian behaviour of blood is also adequate for *high shear rate flow through larger arteries* (Tu and Deville [67], Ponalagusamy [68]).

(iv) The flow is steady, laminar and axially symmetric.

(v) The wall slip is constant.

(vi) The end effects are neglected.

(vii) The solute is completely miscible and its molecular diffusivity is constant. Also, it undergoes a first-order chemical reaction at the capillary wall, which is representative of drugs (pharmacological agents).

2.1. Governing equations

Implementing the above approximations, the momentum equations which govern the flow of blood may be shown to reduce from the Navier–Stokes equations, in a cylindrical coordinate system (r^*, z^*) to:

$$\frac{\partial u^*}{\partial z^*} + \frac{\partial v^*}{\partial r^*} + \frac{v^*}{r^*} = 0, \tag{2.1}$$

$$\rho^*\left[u^*\frac{\partial u^*}{\partial z^*} + v^*\frac{\partial u^*}{\partial r^*}\right] = -\frac{\partial p^*}{\partial z^*} + \mu^*\left[\frac{\partial^2 u^*}{\partial z^{*2}} + \frac{\partial^2 u^*}{\partial r^{*2}} + \frac{1}{r^*}\frac{\partial u^*}{\partial r^*}\right], \tag{2.2}$$

$$\rho^*\left[u^*\frac{\partial v^*}{\partial z^*} + v^*\frac{\partial v^*}{\partial r^*}\right] = -\frac{\partial p^*}{\partial r^*} + \mu^*\left[\frac{\partial^2 v^*}{\partial z^{*2}} + \frac{\partial^2 v^*}{\partial r^{*2}} + \frac{1}{r^*}\frac{\partial v^*}{\partial r^*} - \frac{v^*}{r^{*2}}\right], \tag{2.3}$$

here z^* and r^* are representing the axial and radial coordinates, $p^*(r^*, z^*)$ is the constant pressure, $u^*(r^*, z^*)$ and $v^*(r^*, z^*)$ are the axial and radial velocity components for the blood flow; also, due to the axial symmetry of the flow the velocity component in the azimuthal direction is omitted.

The unsteady two-dimensional convection–diffusion equation for the transport of a reactive solute of concentration C^* can be written as:

$$\frac{\partial C^*}{\partial t^*} + u^*\frac{\partial C^*}{\partial z^*} + v^*\frac{\partial C^*}{\partial r^*} = D\frac{\partial^2 C^*}{\partial z^{*2}} + \frac{D}{r^*}\frac{\partial}{\partial r^*}\left(r^*\frac{\partial C^*}{\partial r^*}\right), \tag{2.4}$$

here, t^* denotes time and D is the molecular diffusivity of the solute which is assumed to be constant.

2.2. Initial and boundary conditions

(i) At the boundary (wall) of the cylindrical capillary, the axial and radial velocities are as follows:

$$u^* = u_s^*, \quad v^* = k(p^* - \alpha) \quad \text{at } r^* = R^*, \tag{2.5}$$

here u_s^* is the slip velocity. Owing to the fact that due to permeability of the capillary wall, consideration of the no-slip condition at the wall may not be valid, the present study on blood flow through a capillary segment has been carried out by paying due attention to slip-velocity at the capillary wall. The boundary condition for the radial velocity v^* follows Starling's law, which states that *the rate of flow per unit area of the wall surface is proportional to the difference in*

fluid pressure inside (p^*) *and outside* (α) *the capillary*; k is the capillary filtration coefficient and is proportional to the capillary wall permeability and the filterable area. The pressure outside the artery is further expressed as $\alpha = \Pi - \Pi_i + p_i$; Π is the osmotic plasma protein pressure; p_i and Π_i are, respectively the *hydrostatic interstitial fluid pressure* and *osmotic pressure of the protein in the interstitial fluid* [69].

Again, the solute is irreversibly and linearly absorbed at the wall with the rate constant Γ^*, and hence:

$$\frac{\partial C^*}{\partial r^*} = -\Gamma^* C^* \quad \text{at } r^* = R^*. \tag{2.6}$$

(ii) Due to the symmetry condition, at the center-line of the capillary we have :

$$\frac{\partial u^*}{\partial r^*} = 0, \qquad \frac{\partial C^*}{\partial r^*} = 0 \quad \text{at } r^* = 0. \tag{2.7}$$

The *transverse velocity* is zero at the center, thus

$$v^* = 0 \quad \text{at } r^* = 0. \tag{2.8}$$

(iii) At the left end (entry) of the capillary i.e., at the axial distance $z^* = -L^*$, the average pressure ($\overline{p}$) is zero, whereas at the opposite end (exit), average pressure is given by:

$$\overline{p} = \frac{P_0 - p_i}{\alpha} \quad \text{at } z^* = L^*, \tag{2.9}$$

where P_0 is the mean pressure over the cross-section of the blood vessel (capillary).

(iv) The solute is released instantaneously uniformly over the cross- section of the capillary and localized near at $z^* = 0$, thus

$$C^* = \frac{Q^*}{\pi R^{*2}} \delta(z^*) \quad \text{at } t^* = 0, \tag{2.10}$$

where δ is the Dirac-delta function.

The asterisk '$*$' over the coordinates and on the physical parameters denotes their dimensional form. Proceeding with the analysis, we next derive the dimensionless form of the above equations via an appropriate set of scaling variables.

2.3. Dimensionless form of equations

Let us consider the following dimensionless quantities:

$$\begin{gathered} t = \frac{Dt^*}{R^{*2}}, \quad r = \frac{r^*}{R^*}, \quad z = \frac{z^*}{L^*}, \quad \lambda = \frac{R^*}{L^*}, \quad u = \frac{u^*}{u_c}, \\ v = \frac{\lambda v^*}{u_c}, \quad p = \frac{p^* - p_i}{\alpha}, \quad C = \frac{C^*}{C_0}, \end{gathered} \tag{2.11}$$

where, $u_c = \alpha R^* \lambda/\mu^*$ is characteristic velocity and C_0 is the reference concentration.

By virtue of Eq. (2.11), the dimensionless forms of Eqs. (2.1)–(2.3) emerge as:

$$\lambda^2 \frac{\partial u}{\partial z} + \frac{\partial v}{\partial r} + \frac{v}{r} = 0, \tag{2.12}$$

$$\mathrm{Re}\left(\lambda^2 u \frac{\partial u}{\partial z} + v \frac{\partial u}{\partial r}\right) = -\frac{\partial p}{\partial z} + \lambda^2 \frac{\partial^2 u}{\partial z^2} + \frac{\partial^2 u}{\partial r^2} + \frac{1}{r}\frac{\partial u}{\partial r}, \tag{2.13}$$

$$\mathrm{Re}\left(\lambda^2 u \frac{\partial v}{\partial z} + v \frac{\partial v}{\partial r}\right) = -\frac{\partial p}{\partial r} + \lambda^2 \frac{\partial^2 v}{\partial z^2} + \frac{\partial^2 v}{\partial r^2} + \frac{1}{r}\frac{\partial v}{\partial r} - \frac{v}{r^2}, \tag{2.14}$$

together with the boundary conditions:

$$u = u_s, \quad v = \lambda^2 \kappa \left(p + \frac{p_i}{\alpha - 1}\right) \quad \text{at } r = 1, \tag{2.15a}$$

$$\frac{\partial u}{\partial r} = 0, \quad v = 0 \quad \text{at } r = 0, \tag{2.15b}$$

$$\overline{p} = 0, \quad \text{at } z = -1, \tag{2.15c}$$

$$\overline{p} = \frac{P_0 - p_i}{\alpha} \quad \text{at } z = 1, \tag{2.15d}$$

here λ is the ratio of radius to length of the capillary, $Re = \rho^* L^* u_c/\mu^*$ is the Reynolds number and $\kappa = k/\lambda^2 \alpha u_c$ is the *filtration coefficient*. It can be assumed that $\mathcal{O}(\lambda^2) = \mathcal{O}(\kappa)$.

Using Eq. (2.11), we have the dimensionless form of the advection diffusion (solute concentration) equation (Eq. (2.4)):

$$\frac{\partial C}{\partial t} + \lambda \mathrm{Pe}\, u(r,z)\frac{\partial C}{\partial z} + \frac{1}{\lambda}\mathrm{Pe}\, v(r,z)\frac{\partial C}{\partial r} = \lambda^2 \frac{\partial^2 C}{\partial z^2} + \frac{1}{r}\frac{\partial}{\partial r}\left(r\frac{\partial C}{\partial r}\right). \tag{2.16}$$

The initial and boundary conditions for the solute concentration become:

$$C(0, r, z) = \lambda \delta(z), \tag{2.17}$$

$$\frac{\partial C}{\partial r} = 0 \quad \text{at } r = 0, \tag{2.18a}$$

$$\frac{\partial C}{\partial r} = -\Gamma C \quad \text{at } r = 1. \tag{2.18b}$$

Here, $\mathrm{Pe} = u_c R^*/D$ is the Péclet number, which measures the relative characteristic time of the diffusion process to the convection process and $\Gamma = \Gamma^* R^*$ is the irreversible reaction rate constant.

3. Solution techniques

3.1. Velocities and pressures

To solve the continuity and momentum Eqs. (2.12)–(2.14) subject to the boundary conditions (2.15), a regular perturbation technique is followed where $\lambda^2 \sim O(\varepsilon)$ is the perturbation parameter. Let us consider the solution of pressure ($p(r,z)$), axial velocity ($u(r,z)$) and transverse velocity ($v(r,z)$) with the following forms:

$$\begin{cases} u = u_0 + \lambda^2 u_1 + \lambda^4 u_2 + O(\lambda^6), \\ v = v_0 + \lambda^2 v_1 + \lambda^4 v_2 + O(\lambda^6), \\ p = p_0 + \lambda^2 p_1 + \lambda^4 p_2 + O(\lambda^6). \end{cases} \tag{3.1}$$

Using Eq. (3.1) in the momentum Eqs. (2.12) – (2.14), we have:

Zeroth-order terms:

$$\frac{\partial v_0}{\partial r} + \frac{1}{r} v_0 = 0, \tag{3.2}$$

$$\mathrm{Re}\left(v_0 \frac{\partial u_0}{\partial r} \right) = -\frac{\partial p_0}{\partial z} + \frac{\partial^2 u_0}{\partial r^2} + \frac{1}{r} \frac{\partial u_0}{\partial r}, \tag{3.3}$$

$$\mathrm{Re}\left(v_0 \frac{\partial v_0}{\partial r} \right) = -\frac{\partial p_0}{\partial r} + \frac{\partial^2 v_0}{\partial r^2} + \frac{1}{r} \frac{\partial v_0}{\partial r} - \frac{v_0}{r^2}, \tag{3.4}$$

the associated boundary conditions:

$$u_0 = u_s, \quad v_0 = 0 \quad \text{at } r = 1, \tag{3.5a}$$

$$\frac{\partial u_0}{\partial r} = 0, \quad v_0 = 0 \quad \text{at } r = 0, \tag{3.5b}$$

$$\overline{p}_0 = 0, \quad \text{at } z = -1, \tag{3.5c}$$

$$\overline{p}_0 = \frac{P_0 - p_i}{\alpha} \quad \text{at } z = 1. \tag{3.5d}$$

Solving the Eqs. (3.2–3.4), using the boundary conditions Eqs. (3.5a)–(3.5d), gives:

$$v_0 = 0, \tag{3.6a}$$

$$p_0 = p_0(z), \tag{3.6b}$$

$$u_0 = -\frac{1}{4} \frac{dp_0}{dz} (1 - r^2) + u_s. \tag{3.6c}$$

First-order terms:

Considering $v_0 = 0$ from Eq. (3.6a), *the first order correction terms* can be written as:

$$\frac{\partial u_0}{\partial z} + \frac{\partial v_1}{\partial r} + \frac{v_1}{r} = 0, \tag{3.7}$$

$$\mathrm{Re}\left(u_0\frac{\partial u_0}{\partial z} + v_1\frac{\partial u_0}{\partial r}\right) = -\frac{\partial p_1}{\partial z} + \frac{\partial^2 u_0}{\partial z^2} + \frac{\partial^2 u_1}{\partial r^2} + \frac{1}{r}\frac{\partial u_1}{\partial r}, \tag{3.8}$$

$$0 = -\frac{\partial p_1}{\partial r} + \frac{\partial^2 v_1}{\partial r^2} + \frac{1}{r}\frac{\partial v_1}{\partial r} - \frac{v_1}{r^2}. \tag{3.9}$$

The boundary conditions are:

$$u_1 = 0, \quad v_1 = \kappa\left(p_0 + \frac{p_i}{\alpha} - 1\right) \quad \text{at } r = 1, \tag{3.10a}$$

$$\frac{\partial u_1}{\partial r} = 0, \quad v_1 = 0 \quad \text{at } r = 0, \tag{3.10b}$$

$$\overline{p}_1 = 0 \quad \text{at } z = \pm 1. \tag{3.10c}$$

Using Eq. (3.6c) in Eq. (3.7) together with boundary condition (3.10b), we have the solution for v_1 as:

$$v_1 = \frac{1}{16}\frac{d^2 p_0}{dz^2}(2r - r^3). \tag{3.11}$$

Now using the Eq. (3.11) in Eq. (3.10a) yields the solution for $p_0(z)$, viz:

$$p_0(z) = C_1 e^{4\sqrt{\kappa}\,z} + C_2 e^{-4\sqrt{\kappa}\,z} + \kappa\left(1 - \frac{p_i}{\alpha}\right). \tag{3.12}$$

Here,

$$C_1 = \frac{1}{2\sinh(8\sqrt{\kappa})}\left\{\left(\frac{P}{\alpha} - \frac{p_i}{\alpha}\right)e^{4\sqrt{\kappa}} + 2\kappa\left(\frac{p_i}{\alpha} - 1\right)\sinh(4\sqrt{\kappa})\right\},$$

$$C_2 = \frac{1}{2\sinh(8\sqrt{\kappa})}\left\{-\left(\frac{P}{\alpha} - \frac{p_i}{\alpha}\right)e^{-4\sqrt{\kappa}} + 2\kappa\left(\frac{p_i}{\alpha} - 1\right)\cosh(4\sqrt{\kappa})\right\}.$$

Finally, the *zeroth-order solutions* for v_0, p_0 and u_0 are obtained from Eq. (3.6) by using Eq. (3.12) as follows:

$$v_0 = 0, \tag{3.13a}$$

$$p_0 = p_0(z) = A(z) + \kappa\left(1 - \frac{p_i}{\alpha}\right), \tag{3.13b}$$

$$u_0 = -\sqrt{\kappa}(1 - r^2)B(z) + u_s, \tag{3.13c}$$

where, $A(z) = C_1 e^{4\sqrt{\kappa}\,z} + C_2 e^{-4\sqrt{\kappa}\,z}$, and $B(z) = C_1 e^{4\sqrt{\kappa}\,z} - C_2 e^{-4\sqrt{\kappa}\,z}$.

Again using Eq. (3.13b) the expression for $v_1(r,z)$ is obtained through Eq. (3.11) as:

$$v_1 = \kappa(2r - r^3)(C_1 e^{4\sqrt{\kappa}\,z} + C_2 e^{-4\sqrt{\kappa}\,z}). \tag{3.14}$$

Now, it is possible to determine the solutions for $p_1(r,z)$ from Eq.(3.9) as we already have v_1 in Eq. (3.14). This gives:

$$p_1 = -4\kappa r^2(C_1 e^{4\sqrt{\kappa}\,z} + C_2 e^{-4\sqrt{\kappa}\,z}) + F_1(z). \tag{3.15}$$

Using u_0, v_1 and p_1 in Eq. (3.8), we have the solution for u_1 with boundary conditions (3.10a, b))

$$\begin{aligned} u_1 = AB\,\mathrm{Re}\,\kappa^{3/2}\left(\frac{1-r^4}{4} - \frac{1-r^6}{18}\right) + 2B\kappa^{3/2}(1-r^4) \\ - \frac{A\,\mathrm{Re}\,u_s\kappa}{4}(1-r^4) - \frac{X(z)}{4}(1-r^2), \end{aligned} \tag{3.16}$$

where $X(z) = F_1'(z) + 16B\kappa^{3/2} - 4\,\mathrm{Re}\,Au_s\kappa + 4\,\mathrm{Re}\,AB\kappa^{3/2}$.

In Eqs. (3.15) and (3.16) there is a common unknown function $F_1(z)$. To find this the continuity equation for the second order approximation in the perturbation series is employed

$$\frac{\partial u_1}{\partial z} + \frac{\partial v_2}{\partial r} + \frac{v_2}{r} = 0. \tag{3.17}$$

The relevant boundary conditions are:

$$v_2 = p_1 \quad \text{at } r = 1, \tag{3.18a}$$

$$v_2 = 0 \quad \text{at } r = 0. \tag{3.18b}$$

The solution of Eq. (3.17) with the boundary condition (3.18b) gives:

$$\begin{aligned} v_2(r,z) = -E\,\mathrm{Re}\,\kappa^2\left[\frac{1}{3}(3r - r^5) - \frac{1}{18}(4r - r^7)\right] - \frac{4A\kappa^2}{3}(3r - r^5) \\ + \frac{B\,\mathrm{Re}\,u_s\kappa^{3/2}}{6}(3r - r^5) + \frac{X'(z)}{16}(2r - r^3), \end{aligned} \tag{3.19}$$

where $E = C_1^2 e^{8\sqrt{\kappa}\,z} + C_2^2 e^{-8\sqrt{\kappa}\,z}$, and $X'(z) = F_1''(z) + 64A\kappa^2 - 16\,\mathrm{Re}\,Bu_s\kappa^{3/2} + 32\,\mathrm{Re}\,E\kappa^2$.

Again using Eq. (3.19) in Eq. (3.18a), we have the differential equation for $F_1(z)$ in the following form:

$$F_1''(z) - 16F_1(z) = \frac{32}{3}\,\mathrm{Re}\,u_s B\kappa^{3/2} - 24\,\mathrm{Re}\,E\kappa^2 - \frac{64}{3}A\kappa(\kappa + 3). \tag{3.20}$$

The solution of $F_1(z)$ is obtained from Eq. (3.20) as follows:

$$F_1(z) = B_1 e^{4z} + B_2 e^{-4z} + \frac{2\kappa^{3/2}}{3(\kappa-1)} \operatorname{Re} u_s B - \frac{3\kappa^2}{2(4\kappa-1)} \operatorname{Re} E - \frac{4\kappa(\kappa+3)}{3(\kappa-1)} A. \tag{3.21}$$

Here B_1 and B_2 are arbitrary constants. Now, Eq. (3.21) is again used in Eq. (3.15), so the expression for p_1 is modified and takes the form:

$$p_1(r,z) = -4A\kappa r^2 + B_1 e^{4z} + B_2 e^{-4z} + \frac{2\kappa^{3/2}}{3(\kappa-1)} \operatorname{Re} u_s B - \frac{3\kappa^2}{2(4\kappa-1)} \operatorname{Re} E - \frac{4\kappa(\kappa+3)}{3(\kappa-1)} A. \tag{3.22}$$

To obtain the arbitrary constants, the cross-sectional average of p_1 is evaluated to make use of the boundary conditions (3.10c). Accordingly, the values of B_1 and B_2 are found to be:

$$\begin{aligned} B_1 = \frac{1}{\sinh(8)} \Bigg[& \frac{2\kappa(5\kappa+3)}{3(\kappa-1)} \{C_1 \sinh(4(\sqrt{\kappa}+1)) - C_2 \sinh(4(\sqrt{\kappa}-1))\} \\ & - \frac{2\kappa^{3/2}}{3(\kappa-1)} \operatorname{Re} u_s \{C_1 \sinh(4(\sqrt{\kappa}+1)) + C_2 \sinh(4(\sqrt{\kappa}-1))\} \\ & + \frac{3\kappa^2}{2(4\kappa-1)} \operatorname{Re}\{C_1^2 \sinh(4(2\sqrt{\kappa}+1)) - C_2^2 \sinh(4(2\sqrt{\kappa}-1))\} \Bigg], \end{aligned} \tag{3.23}$$

$$\begin{aligned} B_2 = \frac{1}{\sinh(8)} \Bigg[& \frac{2\kappa(5\kappa+3)}{3(\kappa-1)} \{C_2 \sinh(4(\sqrt{\kappa}+1)) - C_1 \sinh(4(\sqrt{\kappa}-1))\} \\ & + \frac{2\kappa^{3/2}}{3(\kappa-1)} \operatorname{Re} u_s \{C_1 \sinh(4(\sqrt{\kappa}-1)) + C_2 \sinh(4(\sqrt{\kappa}+1))\} \\ & + \frac{3\kappa^2}{2(4\kappa-1)} \operatorname{Re}\{C_2^2 \sinh(4(2\sqrt{\kappa}+1)) - C_1^2 \sinh(4(2\sqrt{\kappa}-1))\} \Bigg]. \end{aligned} \tag{3.24}$$

Hence, by using the constant values B_1 and B_2 from Eqs. (3.23) and (3.24), the complete solution for F_1 can be obtained from Eq. (3.21), which is used further to get the velocity distribution u_1 from Eq. (3.16). In the present problem we have considered the *axial and radial velocities* up to first-order approximation of the perturbation series. Due to the smaller value of the perturbation parameter, the higher order terms in perturbation series are neglected. Hence, the dispersion theory is based on a *two-dimensional* flow in a permeable capillary. Specifically, this is the novelty of the present work, since the vast majority of other studies

of the Taylor dispersion do not consider two-dimensional flow field for small and moderate times. From the velocity distributions one can see that the flow is characterized by the following three parameters: ratio of radius to length of the capillary λ, the Reynolds number Re and the filtration coefficient κ, respectively. Owing to the consideration of wall permeability, the slip condition is assumed and is denoted by u_s. Now, for $u_s = 0$, $\lambda \to 0$ and $\kappa \to 0$, *zeroth order term* clearly reduces to the Poiseuille flow. Also, one can see the zeroth order terms *are independent* of the Reynolds number. In the upcoming section the axial and radial velocities in Eq. (2.16) are replaced by respective axially average velocity, without violating the overall effect of the convection.

3.2. Solute concentration

Now to solve the convection-diffusion equation (2.16) the generalized dispersion technique of GILL [42] is used. Accordingly, the expansion of concentration $C(t, r, z)$ can be written as:

$$C(t, r, z) = \sum_{k=0}^{\infty} f_k(t, r) \frac{\partial^k C_m}{\partial z^k}, \tag{3.25}$$

where f_k's are the function of t and r to be determined, and $C_m(t, z)$ is the *cross-sectional mean concentration distribution* which is defined as follows:

$$C_m = 2 \int_0^1 Cr \, dr. \tag{3.26}$$

By substituting Eq. (3.25) in Eq. (2.16), the equation for the cross-sectional mean concentration can be written as:

$$\frac{\partial C_m}{\partial t} = \sum_{k=0}^{\infty} M_k(t) \frac{\partial^k C_m}{\partial z^k}. \tag{3.27}$$

For a special case, a particular situation of this Eq. (3.27) is equivalent to the classical Taylor dispersion model. In Eq. (3.27) the M_k's represent various transport coefficients. According to [42], first three transport coefficients are of prime interest, and so the series is truncated up to the 3rd term. This yields:

$$\frac{\partial C_m}{\partial t} = M_0(t) + M_1(t) \frac{\partial C_m}{\partial z} + M_2(t) \frac{\partial^2 C_m}{\partial z^2}, \tag{3.28}$$

where

$$M_0 = -2\Gamma f_0(1, t) - \frac{2\mathrm{Pe}}{\lambda} \int_0^1 r \langle v \rangle_z \frac{\partial f_0}{\partial r} \, dr, \tag{3.29a}$$

$$M_1 = -2\Gamma f_1(1,t) - 2\lambda \mathrm{Pe} \int_0^1 r\,\langle u\rangle_z f_0(r,t)\,dr - \frac{2\mathrm{Pe}}{\lambda}\int_0^1 r\langle v\rangle_z \frac{\partial f_1}{\partial r}\,dr, \tag{3.29b}$$

$$M_2 = \lambda^2 - 2\Gamma f_2(1,t) - 2\lambda \mathrm{Pe} \int_0^1 r\langle u\rangle_z f_1(r,t)\,dr - \frac{2\mathrm{Pe}}{\lambda}\int_0^1 r\langle v\rangle_z \frac{\partial f_2}{\partial r}\,dr. \tag{3.29c}$$

Here, $\langle u\rangle_z$ and $\langle v\rangle_z$ are the cross sectionally average axial and radial velocity, and $\langle\cdot\rangle = \int_{-1}^{1}(\cdot)\,dz$.

The coefficient M_0 is known as the *exchange coefficient*, M_1 is the *advection coefficient*, and M_2 is the *dispersion coefficient*. To understand the transport process further, we will see the influence of velocity profiles together with the effect of various parameters on M_0, M_1 and M_2. It is evident that *generalized dispersion technique of Gill* enables the analysis of the diffusion process in a more precise way. It is also apparent that Eq. (3.29) is coupled with Eq. (3.25) which features the f_k's; the latter can be obtained by substituting Eq. (3.25) in Eq. (2.16). Now, comparing the coefficients of the *longitudinal derivatives*, we have:

$$\frac{\partial f_0}{\partial t} + M_0 f_0 + \left(\frac{\mathrm{Pe}\langle v\rangle_z}{\lambda} - \frac{1}{r}\right)\frac{\partial f_0}{\partial r} - \frac{\partial^2 f_0}{\partial r^2} = 0, \tag{3.30a}$$

$$\frac{\partial f_1}{\partial t} + M_0 f_1 + (M_1 + \lambda \mathrm{Pe}\langle u\rangle_z) f_0 + \left(\frac{\mathrm{Pe}\langle v\rangle_z}{\lambda} - \frac{1}{r}\right)\frac{\partial f_1}{\partial r} - \frac{\partial^2 f_1}{\partial r^2} = 0, \tag{3.30b}$$

$$\frac{\partial f_2}{\partial t} + M_0 f_2 + (M_1 + \lambda \mathrm{Pe}\langle u\rangle_z) f_1 + (M_2 - \lambda^2) f_0 + \left(\frac{\mathrm{Pe}\langle v\rangle_z}{\lambda} - \frac{1}{r}\right)\frac{\partial f_2}{\partial r} - \frac{\partial^2 f_2}{\partial r^2} = 0. \tag{3.30c}$$

The associated initial conditions are:

$$f_k(t=0,r) = \begin{cases} \lambda & \text{for } k = 0. \\ 0 & \text{for } k = 1, 2, \ldots. \end{cases} \tag{3.31}$$

The appropriate boundary conditions are:

$$\frac{\partial f_k}{\partial r} = \begin{cases} 0 & \text{at } r = 0, \\ -\Gamma f_k & \text{at } r = 1, \end{cases} \tag{3.32}$$

where $k = 0, 1, 2$.

As Eqs. (3.29) and (3.30) are coupled with each other, the analytical solution may not be amenable. Thus, a reliable numerical method, namely Crank-Nicolson's finite difference implicit scheme has been followed to solve the system

of equations. The details of the numerical approach are discussed in the Appendix. In the next section, the validity of the numerical scheme for the present model, graphical plots are presented with a detailed elaboration of the computations conducted.

4. Results and discussion

The present study analyses the transport of reactive solute by means of exchange, advection and dispersion coefficients, for blood flow through a permeable capillary. A first-order irreversible reaction is also present at the wall. Considering both the axial and radial velocities is of the prime interest in this work. Due to the consideration of the radial velocity component, the filtration coefficient may control the solute spreading process. The velocity expressions have been derived by the perturbation method and the transport coefficients are computed via the finite difference Crank-Nicolson implicit method. Now, to verify the accuracy of the numerical scheme we examine the effect of axial velocity on the transport processes, for the special scenario when there is *no radial velocity*, i.e., $\lambda \to 0$ (capillary radius becomes vanishingly small) and $\kappa \to 0$ (no filtration coefficient) and compare with earlier studies (see Fig. 2). As expected, all

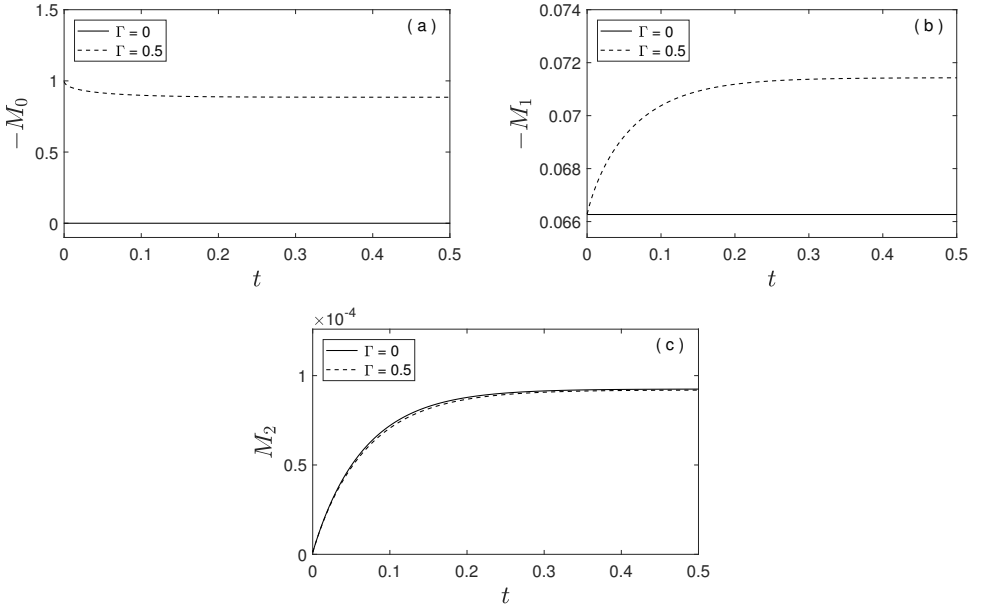

FIG. 2. Temporal variation of exchange coefficient ($-M_0$), convection coefficient ($-M_1$) and dispersion coefficient (M_2) with the wall absorption rate Γ for fixed values of $\beta_1 = 1.39$, $\beta_2 = 0.33$, $\mathrm{Re} = 1$, $u_s = 0$, $\lambda \to 0$ and $\kappa \to 0$, respectively.

the three transport coefficients viz., exchange coefficient, advection coefficient and dispersion coefficient are in excellent agreement with the results reported by Sankarsubramanium and Gill [70] and Rana and Murthy [58] for the Newtonian case. Confidence in the present solutions is therefore established.

In order to appraise the influence of the irreversible reaction rate Γ and the filtration coefficient κ together with the combined effect of radial and axial velocities on the transport processes, it is assumed that $\beta_1 = 1.39$, $\beta_2 = 0.33$, $\mathrm{Re} = 0.09$, $u_s = 0.05$, $\lambda = 0.001$ and these values are prescribed throughout the study. Here, $\beta_1 = p_i/\alpha$, ratio of hydrostatic pressure in the interstitial space to the pressure outside the capillary and $\beta_2 = P/\alpha$, ratio of the mean pressure over the cross-section at the capillary end to the pressure outside the capillary. The results have been evaluated for five different situations as listed in Table 1.

Table 1. Cases and values of controlling parameters deployed in the present study.

Case	Γ	κ	Remark
I	0	0.1	(—) No reaction
II	0.08	0.3	(- - -) Weak absorption
III	1	0.3	(—) Strong absorption
IV	0.3	0.08	(- - -) Low filtration coefficient
V	0.3	1.2	(—) High filtration coefficient

The exchange coefficient evaluates the speed of transport of chemically active solute towards the reactive wall. It is well known from the study of Sankarasubramanian and Gill [70] that the exchange coefficient M_0 occurs due to the presence of chemical reaction at the wall. Also, it was found that M_0 is independent of an axial component of velocity. Nevertheless, it is important to note from Eq. (3.29a), that the exchange coefficient is dependent on the irreversible wall reaction rate and the *radial velocity, but not of the axial velocity.*

Figure 3 displays the variation of negative exchange coefficient with respect to time for the Cases I to V. It can be seen for the Case I, i.e., 'no reaction', that the value of $-M_0$ attains the steady state much faster than the other cases. For Case II, i.e., weak absorption, $-M_0$ takes a relatively small time to reach the steady state. However, for Cases-III to V initially $-M_0$ decreases, with a subsequent slight increment in magnitude and eventually it resumes a decreasing trend. Finally, in all the cases the exchange coefficient is depleted to zero *except for* Case II. Now, the sudden rise of the exchange coefficient after a small interval of time may be associated with the radial velocity. One can also notice that, for the case of *a strong absorption rate* (Case III) the value of the exchange coefficient noticeably exceeds that computed for Case II, i.e., *weak absorption.* This kind of behaviour has also been reported by is also observed by Ng and

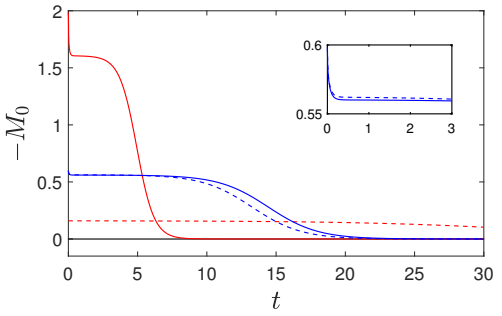

FIG. 3. Temporal variation of exchange coefficient ($-M_0$) for the cases listed in Table 1.

RUDRAIAH [45]. The chemical absorption rate there exerts a substantial influence on the exchange coefficient which agrees with clinical observations. Furthermore, it can be seen that the exchange of solute in between the fluid and solid phases is enhanced with higher values of the filtration coefficient κ, which again is in agreement with physiological observations [69]. It is also apparent from Fig. 3 that for Case III, i.e., strong absorption (—) a significant step change arises at very small times before the eventual steady state is witnessed i.e., there is a dual plateau structure in the plot. For Case II, (- - -) weak absorption, a constant plateau for $-M_0$ attains is observed at all times i.e., the steady state is achieved *immediately and sustained*. Minimum magnitudes of the negative exchange coefficient $-M_0$ are observed for Case I (no reaction). For Cases IV and V i.e., (- - -) low filtration coefficient and (—) high filtration coefficient, there is again a dual plateau topology. The negative exchange coefficient $-M_0$ is invariant with small time values, then drops gradually with further elapse of time, and only then is the steady state distribution achieved. The disparity between negative exchange coefficient $-M_0$ is only observed in the intermediate range of times between Case IV and Case V; clearly Case V produces markedly greater magnitudes of the exchange coefficient in this intermediate time range, due to the greater contribution of the much stronger filtration ($\kappa = 1.2$ for Case V whereas it is very small at $\kappa = 0.08$ for the Case IV) to the solutal dispersion process. The impact of filtration is clearly highlighted, and the inclusion of this effect is strongly justified for more accurate simulations of dispersion in capillary blood flow.

The advection coefficient, which quantifies the process of spreading of solute due to the movement of fluid. Unlike the exchange coefficient, from Eq. (3.29b) it can be seen that the advection coefficient depends on both the velocity components, viz., axial and radial velocities. Figure 4 depicts the negative advection coefficient with respect to time for the list of cases in Table 1. For Case I, $-M_1$ seems to be constant with time, as there is no reaction and the advection speed solely depends on the average velocity. For the Cases II to V, the advection co-

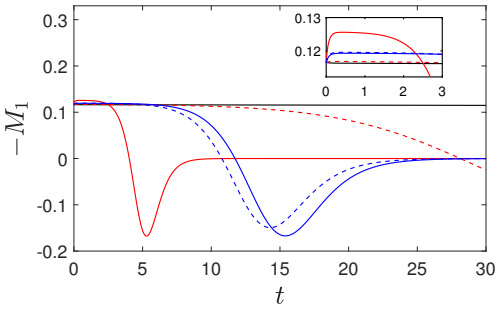

Fig. 4. Temporal variation of advection coefficient ($-M_1$) for the cases listed in Table 1.

efficient *increases* at the initial range $[0, 0.5]$, and then become stable for some time. However, with further progress in time, the advection coefficient drops abruptly and become negative before it finally reaches its steady limit. Similar findings have been observed by Ng and Rudraiah [45] and also Debnath *et. al.* [71] although they employed a different chemical formulation (*reversible and irreversible wall reaction*). The physical cause could be the radial velocity, which acts as a reversible like wall reaction and significantly influences the evolution of the advection coefficient. From Fig. 4 one can see that for Cases III–V, there is no advection coefficient in long-run. Also, it can be seen that the magnitude of $-M_1$ is increasing within a small interval of time due to high absorption as compared to weak absorption, whereas the converse behaviour is computed with variation in the filtration coefficient. Further, because of a *high absorption rate* (Case III) the advection coefficient *approaches the steady state much earlier* than for the case of the weak absorption (Case II). Additionally, as the filtration coefficient κ enhances the advection velocity partially, the advection coefficient thereby attains the steady state slightly faster for the higher values of κ.

The dispersion coefficient, M_2 is the most important parameter for understanding the transport of solute in a solvent flowing through a narrow conduit (capillary) due to both radial diffusion and convection. It measures the dispersion of a solute pulse injected into the flowing stream. Thus, convection has a strong impact in the process of solute spreading. The vast majority of previous studies has considered mostly the influence of an axial velocity component. However, in the present work we have considered both axial and radial velocities, and their dependencies on the dispersion coefficient M_2 is clearly noticed from Eq. (3.29c). The fluctuation of the dispersion coefficient over time is depicted in Fig. 5(a) for the cases mentioned in Table 1. From the figure we can conclude that at the initial stage $[0, 0.5]$ the temporal behaviour of the dispersion coefficient is identical to those cases when there is no radial velocity. For the combined effect of radial and axial velocities, here also the dispersion coefficient is found to be reduced

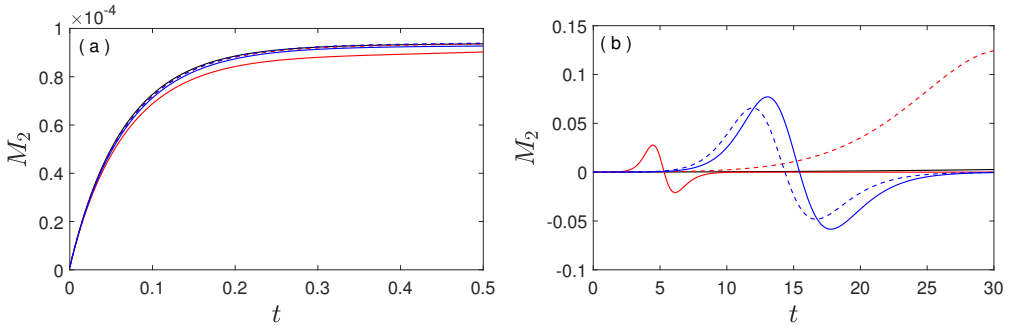

FIG. 5. Temporal variation of dispersion coefficient (M_2) for the cases listed in Table 1.

in magnitude for a high absorption rate relative to the weak absorption rate (Cases II and III, respectively). However, inspection of the profiles for Cases IV and V it can be seen the diffusion processes are accelerated for higher values of the filtration coefficient, which concurs with clinical observations [69].

Interestingly, as time elapses, a dramatic fall in the dispersion coefficient can be seen for the Cases III–V [Fig. 5(b)]. This may be due to the consideration of a radial velocity contribution in the model. At the initial time, *axial diffusion* due to axial convection is the dominating cause of dispersion. However, it is known that after some time, *radial diffusion* controls the diffusion mechanism. At the rear end of the cloud, solute particles attempt to enter the centre part of the solvent flow due to radial diffusion; on the other side radial velocity forces the solute towards the wall. As a consequence of the opposite behaviour of radial diffusion and radial velocity, the solute particles require more time to reach the steady state. More importantly, due to the wall absorption and the filtration coefficient the solute depletion rate at the *front cloud* increases as compared to *rear end*. Thus, large differences in solute concentration between the trailing and leading edges may arise manifesting in a maximum value of the dispersion coefficient. Consequently, the dispersion coefficient will approach negative values after the turning point. After a long duration, the rate of spreading tends to zero and solute dispersion is eliminated in the regime.

Figure 6 shows the variation of transport coefficients with the irreversible wall reaction Γ in the presence of both axial and radial velocities, at a fixed time $t = 10$. Figure 6(a) shows that the negative exchange coefficient increases with increasing irreversible wall reaction, and thereafter a decreasing trend is also observed until it reaches zero. As Γ becomes sufficiently large, reaction at the wall consumes material more rapidly, therefore the concentration of solute at the wall tends to zero. From Fig. 6(b), it can be deduced that the advection coefficient is a decreasing function of Γ, and this depletion continues until the absorption rate exceeds the filtration coefficient $\kappa = 0.3$. After that the convection coefficient increases with Γ and finally reaches an equilibrium state. Figure 6(c) clearly

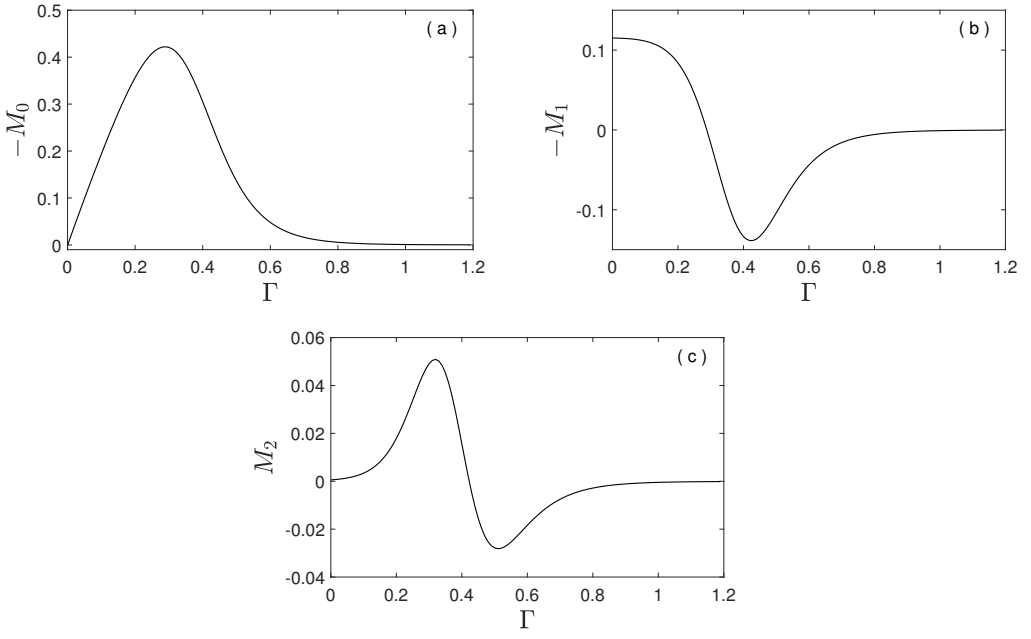

Fig. 6. Variation of the transport coefficients ($-M_0$, $-M_1$ and M_2) with respect to the absorption rate Γ for fixed value of filtration coefficient $\kappa = 0.3$ and $t = 10$.

shows that, the dispersion coefficient increases with Γ, but only for a critical range of Γ values. This interval for Γ is dependent on $\kappa = 0.3$, such that the combined effect of Γ and κ increases the diffusivity of the solute. In the later section of the figure, it is evident that as Γ value exceeds κ, a certain drop of M_2 is induced, and logically after a large Γ is attained, the dispersion coefficient tends to its steady limit.

The axial distribution of mean concentration is derived from the solution of Eq. (3.28) with respect to the initial and boundary conditions. This yields the solution for the solute concentration as:

$$C_m(t,z) = \frac{1}{2Pe\sqrt{\pi\chi}} \exp\left(\xi - \frac{z_1^2}{4\chi}\right), \tag{4.1}$$

where

$$\xi(t) = \int_0^t M_0(\zeta)\, d\zeta, \tag{4.2}$$

$$z_1(t,z) = z + \int_0^t M_1(\zeta)\, d\zeta, \tag{4.3}$$

and

$$\chi(t) = \int_0^t M_2(\zeta)d\zeta. \tag{4.4}$$

Here, the axial mean concentration $C_m(t,z)$ is calculated from Eq. (4.1) by solving Eqs. (4.2) – (4.4) numerically with Simpson's 1/3 rule [72]. In Fig. 7, the *axial distribution of mean concentration* is shown for axial velocity and (axial + radial) velocities at fixed times $t = 0.2$ and $t = 1$. From both figures we can see that the combined effect of both radial and axial velocities *increases the solute diffusivity* as compared to axial velocity alone. It is very important to note that, at small time the differences of a peak height of C_m is significantly lower, whereas at time $t = 1$, the difference is substantial. In other words, one can say at the large time, both axial and radial velocities can play a major role in dispersion of solute, which approximates the actual hemodynamic behaviour [69] more closely than with the simpler Taylor dispersion model.

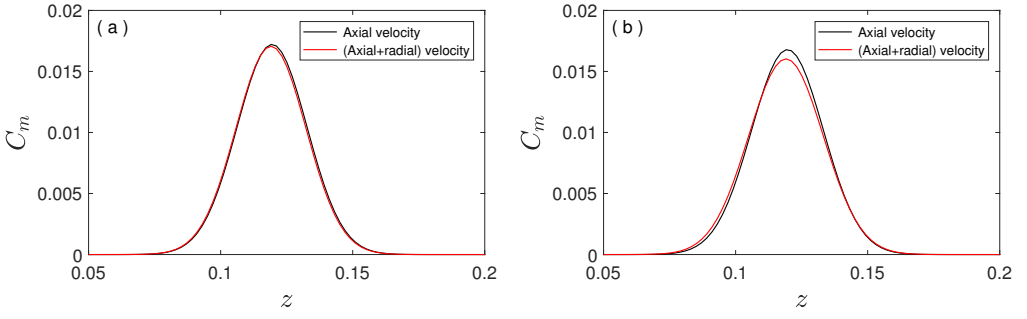

FIG. 7. Axial distribution of mean concentration for the fixed values of $\Gamma = 0.3$ and $\kappa = 0.3$, at time (a) $t = 0.2$, (b) $t = 1$.

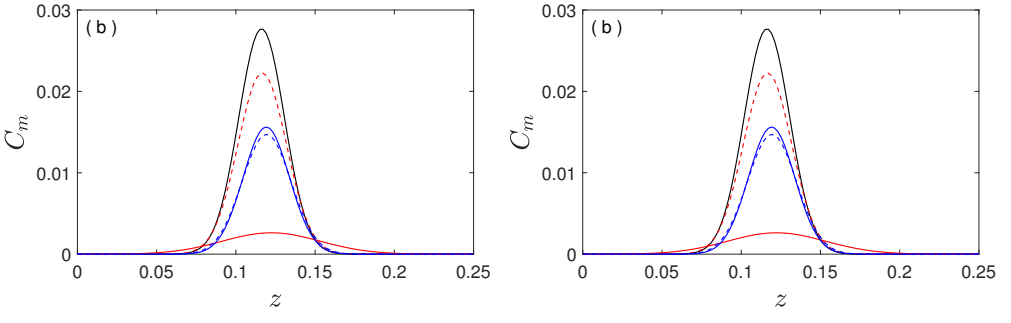

FIG. 8. Axial distribution of mean concentration for the cases listed in Table 1, under the combined effect of axial and radial velocities, at time (a) $t = 1$, (b) $t = 2$.

Figure 8 shows the axial distribution of mean concentration for the cases listed in Table 1 under the consideration of both radial and axial velocities. The results have been plotted for fixed time $t = 1$ and $t = 2$, respectively. For Case I, we can see that the peak height reduces at $t = 2$, which is obvious. Also, from Case I and II, it is clear that with an increase of the irreversible reaction rate Γ the solute diffuses quickly (Fig. 8(a)), and as time increases the peak becomes *much flatter* (Fig. 8(b)). Interestingly, as compared to a low filtration coefficient (Case-IV), the higher filtration coefficient (Case-V) slows down the distribution of mean concentration in the axial direction. The computed behaviour of the filtration coefficient κ on solute dispersion is very significant, and certainly physically viable, as already demonstrated via the earlier graphs showing that increment in κ produces a negative dispersion coefficient.

5. Conclusions

A theoretical study of *reactive solute dispersion in axisymmetric, laminar flow in a permeable capillary*, with a generalized dispersion model has been presented. Blood has been considered to be a Newtonian fluid which is feasible for high shear stress circulatory flows. Also, due to consideration of the endothelium layer encircling the blood vessel, a new parameter, viz., *filtration coefficient*, has been considered in the present study, which affects all the transport coefficients. A regular perturbation method has been implemented to derive velocity and pressure expressions, whereas the Crank–Nicolson implicit finite difference numerical method has been deployed to compute the transport coefficients (M_0 i.e., *exchange coefficient*, M_1 i.e., *advection coefficient*, and M_2 i.e., *dispersion coefficient*). Extensive visualization of different transport coefficients and mean concentrations is presented. The main findings of the present analysis may be summarized as follows:

(a) Radial velocity has no effect on the qualitative behaviour of the transport coefficients at the initial stage of the flow. However, at the transient stage (typically $t \geq 3$, though it may appear earlier then $t = 3$ subject to a different scenario) an influence of the radial velocity observed clearly.
(b) For Cases III–V all the three-transport coefficients tend to zero eventually with large elapse in time.
(c) For high absorption all three transport transport coefficients become zero.
(d) The appearance of radial velocity helps to flatten the breakthrough curve more quickly and become more impactful with a progression in time.
(e) Case I and II demonstrate clearly that with an increase of the irreversible reaction rate the solute diffuses quickly (Fig. 8(a)), and as time increases the peak becomes much flatter.

(f) Compared to a low filtration coefficient (Case IV), the higher filtration coefficient (Case V) decelerates the distribution of mean concentration in the axial direction.

(g) The computed behaviour of the filtration coefficient κ on solute dispersion is effectively very significant and the inclusion of filtration effects is therefore warranted in more realistic blood flow and dispersion models.

The Gill decomposition method has been deployed successfully in the current study. However, attention has been confined to *Newtonian* blood flow i.e., *hemorheology* has been ignored. Future studies may consider several non-Newtonian blood flow models e.g. Sisko's viscoelastic model [72], Eringen's micropolar model [73] or Reiner–Rivlin differential rate-type viscoelastic models [74]. Additionally, the growing popularity of nanoparticles in biomedicine [75, 76] and consideration of more complex geometries (e.g. capillary bifurcations) provides an interesting pathway for studying *generalized dispersion in nanoparticle-doped capillary blood flows in pharmacology.* Efforts in these directions are under consideration and will be reported imminently.

Appendix. Numerical solution by finite difference method

The finite difference Crank–Nicolson implicit scheme [77] is used to solve the following coupled equations along with Eqs. (3.31) and (3.32) to get the transport coefficients $M_k(t)$ ($k = 0, 1,$ and 2).

$$\frac{\partial f_k}{\partial t} + M_0 f_k + (M_1 + \lambda \,\mathrm{Pe}\langle u\rangle_z) f_{k-1} + (M_2 - \lambda^2) f_{k-2} + \left(\frac{\mathrm{Pe}\langle v\rangle_z}{\lambda} - \frac{1}{r}\right)\frac{\partial f_k}{\partial r} - \frac{\partial^2 f_k}{\partial r^2} = 0, \tag{A.1}$$

$$M_k = \lambda^2 \delta_{k2} - 2\Gamma f_k(1,t) - 2\lambda \,\mathrm{Pe} \int_0^1 r\langle u\rangle_z f_{k-1}(r,t)\, dr - \frac{2\mathrm{Pe}}{\lambda}\int_0^1 r\langle v\rangle_z \frac{\partial f_k}{\partial r}\, dr, \tag{A.2}$$

where, $k = 0, 1, 2$ and $f_{-1} = f_{-2} = 0$.

The above equations are discretized by dividing the whole domain ($0 \le r \le 1$) into $(m-1)$ equal grids of length Δr, where each grid point is indicated by the index j. Similarly, the time increment is assumed to be Δt and the corresponding time grid point is denoted by the index i. Therefore, the variables $f_k(r,t)$ and $M_k(t)$ at each grid point are represented by $f_k(j,i)$ and $M_k(i)$ respectively.

Following the above numerical scheme, the Eq. (A.1) becomes a tri-diagonal system of linear equations, which are then solved by a Thomas Algorithm. The scheme is unconditionally stable and by varying the time step and grid spacing, we have assured ourselves of a very good order of accuracy of the results generated for $m = 51$, $\Delta t = 10^{-5}$.

Acknowledgements

The authors are very thankful to editor and referees for their constructive comments and suggestions, which has helped to improve this article.

Conflict of interest

The authors declare no potential conflict of interests.

References

1. S. Middleman, *Transport Phenomena in the Cardiovascular System*, John Wiley & Sons, London, 1972.
2. E.M. Landis, *Handbook of Physiology. Section 2: 'Circulation'*, in *Exchange of Substances Through the Capillary Walls*, vol. 2, American Psychological Society, Washington, 1963.
3. J. Prothero, A.C. Burton, *The physics of blood flow in capillaries: I. The nature of the motion*, Biophysical Journal, **1**, 7, 565–579, 1961.
4. C.C. Michel, *Flows Across the Capillary Wall*, in *Cardiovascular Fluid Dynamics*, vol. 2, Academic Press, New York, 1972.
5. Y.C. Fung, B.W. Zweifach, *Microcirculation: Mechanics of blood flow in capillaries*, Annual Review of Fluid Mechanics, **3**, 1, 189–210, 1971.
6. A.C.L. Barnard, L. Lopez, J.D. Hellums, *Basic theory of blood flow in capillaries*, Microvascular Research, **1**, 1, 23–34, 1968.
7. T.W. Secomb, R. Skalak, N. Özkaya, J.F. Gross, *Flow of axisymmetric red blood cells in narrow capillaries*, Journal of Fluid Mechanics, **163**, 405–423, 1986.
8. M. El-Shahed, *Blood flow in a capillary with permeable wall*, Physica A: Statistical Mechanics and its Applications, **338**, 3, 544–558, 2004.
9. G. Fibich, Y. Lanir, N. Liron, *Mathematical model of blood flow in a coronary capillary*, American Journal of Physiology-Heart and Circulatory Physiology, **265**, 5, H1829–H1840, 1993.
10. M. Soltani, P. Chen, *Numerical modeling of interstitial fluid flow coupled with blood flow through a remodeled solid tumor microvascular network*, PLOS ONE, **8**, 6, e67025, 2013.
11. M. Peyrounette, Y. Davit, M. Quintard, S. Lorthois, *Multiscale modelling of blood flow in cerebral microcirculation: details at capillary scale control accuracy at the level of the cortex*, PLOS ONE, **13**, 1, e0189474, 2018.

12. D. TRIPATHI, S. BHUSHAN, O.A. BÉG, *Analytical study of electro-osmosis modulated capillary peristaltic hemodynamics*, Journal of Mechanics in Medicine and Biology, **17**, 3, 1750052, 2017.

13. C. POZRIKIDIS, *Computational Hydrodynamics of Capsules and Biological Cells*, CRC Press, New York, 2010.

14. D.A. FEDOSOV, J. FORNLEITNER, G. GOMPPER, *Margination of white blood cells in microcapillary flow*, Physical Review Letters, **108**, 2, 028104, 2012.

15. K. BORYCZKO, W. DZWINEL, D.A. YUEN, *Dynamical clustering of red blood cells in capillary vessels*, Journal of Molecular Modeling, **9**, 1, 16–33, 2003.

16. J.L. MCWHIRTER, H. NOGUCHI, G. GOMPPER, *Flow-induced clustering and alignment of vesicles and red blood cells in microcapillaries*, PNAS, **106**, 15, 6039–6043, 2009.

17. J.D. DURRANT, J.A. MCCAMMON, *Molecular dynamics simulations and drug discovery*, BMC Biology, **9**, 1, 71, 2011.

18. E. VENDEL, V. ROTTSCHÄFER, E.C.M. DE LANGE, *The need for mathematical modelling of spatial drug distribution within the brain*, Fluids Barriers CNS, **16**, 1, 12, 2019.

19. N. SAFAEIAN, T. DAVID, *A computational model of oxygen transport in the cerebrocapillary levels for normal and pathologic brain function*, Journal of Cerebral Blood Flow and Metabolism, **33**, 10, 1633–1641, 2013.

20. A. VIKHANSKY, W. WANG, *Taylor dispersion in finite-length capillaries*, Chemical Engineering Science, **66**, 4, 642–649, 2011.

21. M. SAADATMAND, T. ISHIKAWA, N. MATSUKI, M.J. ABDEKHODAIE, Y. IMAI, H. UENO, T. YAMAGUCHI, *Fluid particle diffusion through high-hematocrit blood flow within a capillary tube*, Journal of Biomechanics, **44**, 1, 170–175, 2011.

22. P.N. TANDON, M. MISRA, A. CHAURASIA, *A model for the nutritional transport in capillary-tissue exchange system*, International Journal of Bio-Medical Computing, **37**, 1, 19–28, 1994.

23. T.W. SECOMB, R. HSU, A.R. PRIES, *A model for red blood cell motion in glycocalyx-lined capillaries*, American Journal of Physiology-Heart and Circulatory Physiology, **274**, 3, H1016–H1022, 1998.

24. E.M. RENKIN, *Transport of potassium-42 from blood to tissue in isolated mammalian skeletal muscles*, American Journal of Physiology, **197**, 6, 1205–1210, 1959.

25. G.I. TAYLOR, *Dispersion of soluble matter in solvent flowing slowly through a tube*, Proceedings of the Royal Society A, **219**, 1137, 186–203, 1953.

26. R. ARIS, *On the dispersion of a solute in a fluid flowing through a tube*, Proceedings of the Royal Society A, **235**, 1200, 67–77, 1956.

27. B.S. MAZUMDER, S.K. DAS, *Effect of boundary reaction on solute dispersion in pulsatile flow through a tube*, Journal of Fluid Mechanics, **239**, 523–549, 1992.

28. B.S. MAZUMDER, K.K. MONDAL, *On solute transport in oscillatory flow through an annular pipe with a reactive wall and its application to a catheterized artery*, Quarterly Journal of Mechanics and Applied Mathematics, **58**, 3, 349–365, 2005.

29. B.S. MAZUMDER, S. PAUL, *Dispersion of reactive species with reversible and irreversible wall reactions*, Heat Mass Transfer, **48**, 6, 933–944, 2012.

30. S. DEBNATH, A.K. SAHA, B.S. MAZUMDER, A.K. ROY, *Dispersion phenomena of reactive solute in a pulsatile flow of three-layer liquids*, Physics of Fluids, **29**, 9, 097107, 2017.

31. S. Debnath, S. Paul, A. Roy, *Transport of reactive species in oscillatory annular flow*, Journal of Applied Fluid Mechanics, **11**, 2, 2018.

32. S. Debnath, A.K. Saha, B.S. Mazumder, A.K. Roy, *Hydrodynamic dispersion of reactive solute in a Hagen–Poiseuille flow of a layered liquid*, Chinese Journal of Chemical Engineering, **25**, 7, 862–873, 2017.

33. S. Debnath, A.K. Saha, B.S. Mazumder, A.K. Roy, *On transport of reactive solute in a pulsatile Casson fluid flow through an annulus*, International Journal of Computational Mathematics, **97**, 11, 2303–2319, 2020.

34. S. Debnath, A.K. Saha, B.S. Mazumder, A. Roy, *Dispersion of reactive species in Casson fluid flow*, Indian Journal of Pure and Applied Mathematics, **51**, 4, 1451–1469, 2020.

35. A.K. Roy, A.K. Saha, S. Debnath, *On dispersion in oscillatory annular flow driven jointly by pressure pulsation and wall oscillation*, Journal of Applied Fluid Mechanics, **10**, 5, 1487–1500, 2017.

36. A. K. Roy, A. K. Saha, S. Debnath, *Unsteady convective diffusion with interphase mass transfer in Casson liquid*, Periodica Polytechnica Chemical Engineering, **62**, 2, 215–223, 2018.

37. A.K. Roy, A.K. Saha, R. Ponalagusamy, S. Debnath, *Mathematical model on magneto-hydrodynamic dispersion in a porous medium under the influence of bulk chemical reaction*, Korea Australia Rheology Journal, **32**, 4, 287–299, 2020.

38. L. Zhang, M. A. Hesse, M. Wang, *Transient solute transport with sorption in Poiseuille flow*, Journal of Fluid Mechanics, **828**, 733–752, 2017.

39. G. Li, W. Jiang, P. Wang, J. Guo, Z. Li, G. Chen, *Concentration moments based analytical study on taylor dispersion: Open channel flow driven by gravity and wind*, Journal of Hydrology, **562**, 244–253, 2018.

40. S. Debnath, K. Ghoshal, *Transport of reactive species in oscillatory Couette–Poiseuille flows subject to homogeneous and heterogeneous reactions*, Applied Mathematics and Computation, **385**, 125387, 2020.

41. M. Guan, L. Zeng, C. Li, X. Guo, Y. Wu, P. Wang, *Transport model of active particles in a tidal wetland flow*, Journal of Hydrology, **593**, 125812, 2021.

42. W. N. Gill, *A note on the solution of transient dispersion problems*, Proceedings of the Royal Society A, **298**, 1454, 335–339, 1967.

43. A. Sarkar, G. Jayaraman, *The effect of wall absorption on dispersion in oscillatory flow in an annulus: Application to a catheterized artery*, Acta Mechanica, **172**, 3, 151–167, 2004.

44. P. Nagarani, G. Sarojamma, G. Jayaraman, *Effect of boundary absorption in dispersion in Casson fluid flow in a tube*, Annals of Biomedical Engineering, **32**, 5, 706–719, 2004.

45. C.-O. Ng, N. Rudraiah, *Convective diffusion in steady flow through a tube with a retentive and absorptive wall*, Physics of Fluids, **20**, 7, 073604, 2008.

46. S. Paul, C.-O. Ng, *On the time development of dispersion in electroosmotic flow through a rectangular channel*, Acta Mechanica Sinica, **28**, 3, 631–643, 2012.

47. W.-Q. Jiang, P. Wang, G. Chen, *Concentration distribution of environmental dispersion in a wetland flow: extended solution*, Journal of Hydrology, **549**, 340–350, 2017.

48. S. Debnath, A.K. Saha, A.K. Roy, *A study on solute dispersion in a three layer blood-like liquid flowing through a rigid artery*, Periodica Polytechnica Mechanical Engineering, **61**, 3, 173–183, 2017.

49. S. Debnath, W. Jiang, M. Guan, G. Chen, *Effect of ring-source release on dispersion process in Poiseuille flow with wall absorption*, Physics of Fluids, **34**, 2, 027106, 2022.

50. J. Rana, P. Murthy, *Unsteady solute dispersion in non-Newtonian fluid flow in a tube with wall absorption*, Proceedings of the Royal Society A, **472**, 2193, 20160294, 2016.

51. J. Rana, P. Murthy, *Unsteady solute dispersion in small blood vessels using a two-phase Casson model*, Proceedings of the Royal Society A, **473**, 2204, 20170427, 2017.

52. W.Q. Jiang, G.Q. Chen, *Solution of Gill's generalized dispersion model: solute transport in Poiseuille flow with wall absorption*, International Journal of Heat and Mass Transfer, **127**, 34–43, 2018.

53. A.K. Roy, S. Shaw, *Shear augmented microvascular solute transport with a two-phase model: Application in nanoparticle assisted drug delivery*, Physics of Fluids, **33**, 3, 031904, 2021.

54. J. Guo, W. Jiang, G. Chen, Z. Li, N.S. Alharbi, M. Wakeel, *Solute dispersion in an open channel turbulent flow: Solution by a generalized model*, Journal of Hydrology, **604**, 127239, 2022.

55. C.-O. Ng, *Dispersion in steady and oscillatory flows through a tube with reversible and irreversible wall reactions*, Proceedings of the Royal Society A, **462**, 2066, 481–515, 2006.

56. Z. Wu, G. Chen, *Approach to transverse uniformity of concentration distribution of a solute in a solvent flowing along a straight pipe*, Journal of Fluid Mechanics, **740**, 196–213, 2014.

57. A.K. Roy, A.K. Saha, S. Debnath, *Effect of multiple reactions on the transport coefficients in pulsatile flow through an annulus*, International Communications in Heat and Mass Transfer, **110**, 104369, 2020.

58. J. Rana, P.V.S.N. Murthy, *Solute dispersion in pulsatile Casson fluid flow in a tube with wall absorption*, Journal of Fluid Mechanics, **793**, 877–914, 2016.

59. A.K. Roy, O.A. Bég, A.K. Saha, J.V.R. Murthy, *Taylor dispersion in non-Darcy porous media with bulk chemical reaction: a model for drug transport in impeded blood vessels*, Journal of Engineering Mathematics, **127**, 1, 24, 2021.

60. A.K. Roy, O.A. Bég, *Mathematical modelling of unsteady solute dispersion in two-fluid (micropolar-Newtonian) blood flow with bulk reaction*, International Communications in Heat and Mass Transfer, **122**, 105169, 2021.

61. P. Das, Sarifuddin, J. Rana, P.K. Mandal, *Solute dispersion in transient Casson fluid flow through stenotic tube with exchange between phases*, Physics of Fluids, **33**, 6, 061907, 2021.

62. B. Wang, W. Jiang, G. Chen, L. Tao, Z. Li, *Vertical distribution and longitudinal dispersion of gyrotactic microorganisms in a horizontal plane Poiseuille flow*, Physical Review Fluids, **6**, 5, 054502, 2021.

63. H.C. Chu, S. Garoff, T.M. Przybycien, R.D. Tilton, A.S. Khair, *Dispersion in steady and time-oscillatory two-dimensional flows through a parallel-plate channel*, Physics of Fluids, **31**, 2, 022007, 2019.

64. M. Nakad, T. Witelski, J.-C. Domec, S. Sevanto, G. Katul, *Taylor dispersion in osmotically driven laminar flows in phloem*, Journal of Fluid Mechanics, **913**, 2021.

65. Q. Long, X. Xu, K. Ramnarine, P. Hoskins, *Numerical investigation of physiologically realistic pulsatile flow through arterial stenosis*, Journal of Biomechanics, **34**, 10, 1229–1242, 2001.

66. H. Goldsmith, R. Skalak, *Hemodynamics*, Annual Review of Fluid Mechanics, **7**, 1, 213–247, 1975.

67. C. Tu, M. Deville, *Pulsatile flow of non-Newtonian fluids through arterial stenoses*, Journal of Biomechanics, **29**, 7, 899–908, 1996.

68. R. Ponalagusamy, *Mathematical analysis on effect of non-Newtonian behavior of blood on optimal geometry of microvascular bifurcation system*, Journal of the Franklin Institute, **349**, 9, 2861–2874, 2012.

69. Y.C. Fung, *Biomechanics: Motion, Flow, Stress, and Growth*, Springer, New York, 1990.

70. R. Sankarasubramanian, W.N. Gill, *Unsteady convective diffusion with interphase mass transfer*, Proceedings of the Royal Society A, **333**, 1592, 115–132, 1973.

71. S. Debnath, A.K. Saha, B.S. Mazumder, A.K. Roy, *Transport of a reactive solute in a pulsatile non-Newtonian liquid flowing through an annular pipe*, Journal of Engineering Mathematics, **116**, 1, 1–22, 2019.

72. K.S. Mekheimer, M.A. El Kot, *Mathematical modelling of unsteady flow of a Sisko fluid through an anisotropically tapered elastic arteries with time-variant overlapping stenosis*, Applied Mathematical Modelling, **36**, 11, 5393–5407, 2012.

73. B. Vasu, A. Dubey, O. A. Bég, R.S.R. Gorla, *Micropolar pulsatile blood flow conveying nanoparticles in a stenotic tapered artery: NON-Newtonian pharmacodynamic simulation*, Computers in Biology and Medicine, **126**, 104025, 2020.

74. A. Zaman, N. Ali, O.A. Bég, M. Sajid, *Heat and mass transfer to blood flowing through a tapered overlapping stenosed artery*, International Journal of Heat and Mass Transfer, **95**, 1084–1095, 2016.

75. J. Tripathi, B. Vasu, O.A. Bég, R.S.R. Gorla, *Unsteady hybrid nanoparticle-mediated magneto-hemodynamics and heat transfer through an overlapped stenotic artery: Biomedical drug delivery simulation*, Proceedings of the Institution of Mechanical Engineers, Part H: Journal of Engineering in Medicine, **235**, 10, 1175–1196, 2021.

76. A. Dubey, V.B., O.A. Bég, R.S.R. Gorla, *Finite element computation of magneto-hemodynamic flow and heat transfer in a bifurcated artery with saccular aneurysm using the Carreau-Yasuda biorheological model*, Microvascular Research, **138**, 104221, 2021.

77. S.C. Chapra, R.P. Canale, *Numerical Methods for Engineers*, vol. 1221, 8th ed., McGraw Hill, New York, 2011.

Received December 14, 2021; revised version April 24, 2022.
Published online May 17, 2022.